Journal of Neuro-Oncology **50:** 215–226, 2000.

Laboratory Investigation

Relationships between choline magnetic resonance spectroscopy, apparent diffusion coefficient and quantitative histopathology in human glioma

Rakesh K. Gupta[1], Timothy F. Cloughesy[2,3], Usha Sinha[1], Justine Garakian[4], Jorge Lazareff[5], Gregory Rubino[5], Lisa Rubino[5], Donald P. Becker[5], Harry V. Vinters[4,6] and Jeffry R. Alger[1,3,6]
[1]*Department of Radiological Sciences,* [2]*Department of Neurology,* [3]*Jonsson Comprehensive Cancer Center,* [4]*Department of Pathology and Laboratory Medicine (Neuropathology),* [5]*Department of Surgery, Division of Neurosurgery,* [6]*Brain Research Institute, University of California, Los Angeles, CA, USA*

Key words: brain, brain tumors, MRI, MR spectroscopy, diffusion imaging, glioma

Summary

This study sought to correlate quantitative presurgical proton magnetic resonance spectroscopic imaging (^{1}H-MRSI) and diffusion imaging (DI) results with quantitative histopathological features of resected glioma tissue. The primary hypotheses were (1) glioma choline signal correlates with cell density, (2) glioma apparent diffusion coefficient (ADC) correlates inversely with cell density, (3) glioma choline signal correlates with cell proliferative index. Eighteen adult glioma patients were preoperatively imaged with ^{1}H-MRSI and DI as part of clinically-indicated MRI evaluations. Cell density and proliferative index readings were made on surgical specimens obtained at surgery performed within 12 days of the radiologic scans. The resected tissue location was identified by comparing preoperative and postoperative MRI. The tumor to contralateral normalized choline signal ratio (nCho) and the ADC from resected tumor regions were measured from the preoperative imaging data. Counts of nuclei per high power field in 5–10 fields provided a quantitative measure of cell density. MIB-1 immunohistochemistry provided an index of the proportion of proliferating cells. There was a statistically significant inverse linear correlation between glioma ADC and cell density. There was also a statistically significant linear correlation between the glioma nCho and the cell density. The nCho measure did not significantly correlate with proliferative index. The results indicate that both ADC and spectroscopic choline measures are related to glioma cell density. Therefore they may prove useful for differentiating dense cellular neoplastic lesions from those that contain large proportions of acellular necrotic space.

Introduction

Proton magnetic resonance spectroscopic imaging (^{1}H-MRSI) and diffusion magnetic resonance imaging (DI) have probable value in the clinical assessment of human intracranial glioma, yet little effort has been made to relate the ^{1}H-MRSI and DI features seen in glioma with cellular characteristics identifiable on quantitative histopathology.

^{1}H-MRSI provides tomographic measures of the magnetic resonance spectroscopic signal intensities produced by several low molecular weight tissue constituents with a volume resolution that can be as fine as 0.34 cc [1–6]. Numerous studies have demonstrated that, for glioma evaluation, the choline signal is one of the most significant of the detectable spectroscopy signals [2–13]. Its relative elevation in cerebral neoplastic tissue has been frequently reported. The association between increased choline signal intensity and malignant degeneration or progression of human glioma has been demonstrated [4,5]. There is also a growing body of investigation in which spectroscopic observables, particularly the choline signal, are used to assess therapeutic response [5,12,13]. All of these avenues are being pursued without a firm understanding of what underlying biophysical or biochemical features are responsible for glioma choline signal elevation and its changes. Cell culture studies have

implicated enhanced 'membrane turnover' associated with neoplastic transformation and cellular proliferation as a key biochemical component responsible for choline signal elevation [14]. However, there remains a poor understanding of how the known variability in cell density (micronecrosis) modulates the biochemical effects in human intracranial glioma.

DI enables the self-diffusion properties of tissue water to be imaged [15]. It has been used most frequently in the evaluation of acute stroke [16]; however exploratory investigations of human glioma have also appeared [17–22]. These have inferred (from imaging without a histopathological correlation) that Apparent Diffusion Coefficient (ADC) imaging permits the topospecific identification of the unique histopathologic components of glioma which may not be clearly distinguishable on conventional MRI; higher ADC suggests lower cell density (e.g. cyst, micronecrosis, edema) while lower ADC values suggest solid tumor. This inferred finding has not yet been tested through a correlative imaging/histopathological study. A recent contribution described the relationship between choline ^{1}H-MRSI signal intensity and the ADC in human glioma [21]. This study found a statistically significant inverse correlation between ADC and choline signal intensity in human glioma and, thereby, provided preliminary evidence for a self-consistent picture in which both the ADC and the choline signal intensity are closely related to cell density. However, this study did not include a histopathological correlation to support this hypothetical relationship between ADC, choline signal and cell density.

In the present investigation we directly studied the relationship between imaging parameters and histopathologic parameters. The parameters of interest were choline signal intensity, ADC, tumor cell density and cell proliferative index. The primary hypotheses that guided the data evaluation were:

1. A direct correlation exists between choline signal intensity and cell density because the metabolites that generate the choline signal are associated with the cells rather than the extracellular space;
2. An inverse correlation exists between ADC and cell density due to a presumed decreased amount of highly mobile extracellular water in dense tumor tissues;
3. A direct correlation exists between choline signal intensity and cell proliferative index because 'membrane turnover' and, therefore, choline metabolites are expected to be elevated in proliferating cells.

The use of stereotactic biopsy was considered for this study as means of obtaining the maximum possible correlation between imaging and histopathological data. However this proved not to be possible because of the relative infrequency of stereotactic biopsy at our institution. These considerations led to the design of a statistically valid procedure for testing the hypotheses using open resections.

Materials and methods

Overall design

Eighteen glioma patients were presurgically scanned using an integrated magnetic resonance examination which included conventional MRI, ^{1}H-MRSI and DI. The patient group included 14 males and 4 females, aged 28–62 years. All patients had surgery within 12 days after the imaging study. Some of the patients had newly diagnosed glioma without previous treatment (excepting steroids), while others had surgery for recurrent or progressive glioma. Table 1 provides the histopathological diagnoses using Daumas–Duport criteria [23]. Seventeen patients underwent postsurgical followup conventional MRI scanning within two weeks of surgery. One patient had a postsurgical CT scan due to postsurgical complications and a followup MRI within 30 days. For each patient presurgical and postsurgical anatomical imaging studies (MRI or CT) were compared by an experienced radiologist (RG) to identify the tissue that was resected. The volume average ADC and volume average spectroscopic choline signal intensity over the resected tissue were then determined from the preoperative imaging study.

Cell density assays of the resected tissues were obtained by nuclear counts. MIB-1 immunohistochemistry [24] was used to obtain the cell proliferative index. Linear regression techniques were used to test for the hypothesized relationships between measured parameters.

MRI

The patients were scanned using a 1.5 Tesla MRI system (General Electric Signa 5× Echospeed). MRI, ^{1}H-MRSI and DI were performed during the same scanning session without repositioning the patient. The conventional imaging included pre- and postcontrast T1-weighted axial imaging

Table 1. Summary of measurements

Pt	Diagnosis	Diagnostic classification	Average nuclei count (thousands per high power field)	Average proliferation index (MIB-1)	Average ADC μm^2/sec	Average nCho
1	GBM	G	1.00	17.7	1025	1.7
2	GBM	G	0.27	4.9	1423	1.3
3	LGA	A	0.57	4.6	1142	1.4
4	GBM	G	1.61	10.4	1245	3.4
5	GBM	G	0.62	6.1	1362	0.8
6	GBM	G	0.83	11.0	1375	0.6
7	LGO	O	1.65	2.4	1226	5.6
8	LGO	O	1.82	8.8	1013	2.7
9	LGA	A	1.03	2.8	1443	1.5
10	LGO	O	1.63	14.3	740	6.5
11	GBM	G	1.91	12.3	985	3.5
12	MOA	M	1.54	8.9	1043	2.9
13	GBM	G	0.58	8.5	1234	1.8
14	AA	A	1.09	5.5	1101	8.6
15	GBM	G	0.79	0.9	1380	1.6
16	AO	O	1.36	2.4	1084	4.1
17	GBM/O	M	3.31	13.7	840	6.3
18	MMG	M	1.05	5.6	1047	4.8

Abbreviations: GBM: Gliobastoma Multiforme; GA: Low Grade Astrocytoma; LGO: Low Grade Oligodendroglioma; MOA: Mixed Oligodendroglioma and Astrocytoma; AA: Anaplastic Astrocytoma; AO: 4 Anaplastic Oligodendroglioma; GBM/O: Gliobastoma Multiforme with a major Oligodendroglial component; MMG: Malignant Mixed Glioma; Pt: Patients. *Diagnostic Classifications*: G: GBM; A: Astrocytoma; O: Oligodendroglioma; M: Mixed.

(TR/TE/NEX = 500/8/2, slice thickness = 3 mm, slice gap = 0, 192 × 256 matrix) together with fast spin echo proton density weighted and T2 weighted axial imaging (TR/TE1/TE2/NEX = 6000/14/126/2, slice thickness = 3 mm, slice gap = 0, 192 × 256 matrix). MRI contrast agent was administered after the ^{1}H-MRSI and DI scanning in all cases. All MRI scanning volumetric prescriptions (slice locations, slice thickness, field-of-view, field-of-view center) were prospectively defined so that images of different types (e.g. ADC, ^{1}H-MRSI, MRI) were collected in registration.

^{1}*H-MRSI*

Axial 1^{1}H-MRSI was performed using a three slice multislice technique with TR/TE = 2300/272, a 24 × 24 phase encoding array, a slice thickness of 12 mm, a slice gap of 0 mm and a field-of-view of 240 mm. This ^{1}H-MRSI technique provides T2-weighted proton magnetic resonance spectra from an array of voxels having nominal dimensions of 10 × 10 × 12 mm^3 from each of the three defined slices. Water suppression was accomplished using three frequency selective radiofrequency pulses in concert with gradient pulses to destroy coherent water magnetization at the beginning of each pass through the pulse sequence. Lipid suppression was achieved using the short-tau-inversion-recovery method with TI of 170 msec. This methodology was chosen because, in our hands, it is robust and the data it produces are relatively easily quantified. The ^{1}H-MRSI data from each spectroscopic imaging slice were reconstructed using 3-dimensional (two spatial and one frequency dimensions) fourier transform following sine-bell spatial filtering and 2.0 Hz lorentzian time domain filtering. This produced a two-dimensional array of voxel frequency spectra from each of the three imaged slices. Topographically registered conventional MRI scans were created by summing the four 3 mm thick scans which coincided with each spectroscopic imaging slice. Topographically registered ADC scans were obtained by collecting the DI scans with a slice thickness of 12 mm using a slice location prescription that matched the spectroscopic imaging prescription. Therefore, the tissue location which produced each voxel frequency spectrum could be identified on any

of the topographically registered MRIs, including the ADC images. Frequency spectra from each of the intracranial voxels were frequency-referenced by identifying characteristic spectroscopic signals (e.g. NAA, choline and creatine). Voxel spectra were then baseline corrected using a polynomial fitting procedure to fit the baseline in frequency regions having no signals. Integrated magnitude signal intensities (hereafter referred to as 'signal intensities') of the choline, N-acetylaspartate (NAA) and creatine signals were obtained by integration of a 0.1 ppm frequency region around the respective signal maxima in each of the voxels. Lactate and lipid signals were infrequently detected and were, therefore not analyzed further. Signal intensities were color coded for display as spectroscopic images. Choline signal alterations associated with tumor were quantified using the 'normalized choline' signal approach. For this method of choline signal quantification, the choline signal in the tissue of interest is measured as is the choline signal generated by contralaterally homologous region that appears normal on conventional MRI. The lesion choline signal measure is divided by the contralateral choline signal measure. This ratio is designated with the abbreviation nCho in the remainder of the paper. In this manner, the lesion choline signal measure is 'normalized' to that produced by normal tissue in the contralateral hemisphere. This is necessary because MRI instruments provide no reliable absolute measure of signal intensity. Between-subject analyses, therefore, require calibration against some other 'standard signal', which in this case was the choline signal produced by the normal appearing tissue in the contralateral hemisphere. The choline signal intensities arising from spectroscopic imaging voxels located in the ultimately resected regions were read. Readings were also made from voxels located in contralateral normal appearing regions and the ratio of the tumor to contralateral signal intensity was calculated for each patient. The sampling was performed as follows. The radiologist (RG) retrieved the postoperative and the preoperative MRI studies. These were displayed beside each other to permit him to determine what specific tissue volume was resected. A combination of T1-weighted and T2-weighted MRI were used. The preoperative MRI and the ^{1}H-MRSI were collected during the same scan session and were prescribed such that they were volumetrically registered with each other. The radiologist sampled the preoperative ^{1}H-MRSI data that were produced by the tissue that was subsequently resected using 'MRI guidance'. This was done using software of our own design that permits one to point at the resected tissue location on the MRI and to display the ^{1}H-MRSI data produced by that tissue location. However locations that included obvious cystic regions on MRI were not sampled as these tend to produce no spectroscopic signals of any type.

DI

A diffusion-weighted spin echo-planar imaging technique was used. To simplify image manipulation, diffusion scans were performed using 12 mm thick slices prescribed to match the ^{1}H-MRSI slice prescription. The diffusion sensitization parameters were: $\delta = 35$ msec (all three axes), $\Delta = 37.6$ msec in the read (x) and phase (y) directions, $\Delta = 40.2$ msec in the slice select (z) direction, diffusion-weighting gradient pulse amplitudes $= 0.0, 4.0, 8.0, 12.0$, and 16.0 μT/mm. The corresponding 'b values' ranged from 0 to 940 sec/mm^2 along the read and phase directions and from 0 to 1112 sec/mm^2 along the slice select axis. The b value calculation took into account both the diffusion sensitizing gradient pulses and the imaging gradient pulses. Gradient tuning was performed for the $b = 0$ images only; all the other diffusion-weighted images were acquired at the same settings. Image distortions were reduced by using the minimum possible TE with a half-fourier acquisition. Diffusion-weighted echo-planar images were acquired with successive sensitization in the x, y and z directions. Image intensities in the diffusion-weighted images (5b values, 3 directions) were log-linear fit on a pixel-by-pixel basis to generate three directional ADC images (ADC_{xx}, ADC_{yy}, ADC_{zz}). The approximate ADC trace image was then calculated as $1/3\{ADC_{xx} + ADC_{yy} + ADC_{zz}\}$. In the remainder of this paper, the 'ADC trace' will be denoted as 'ADC'. Quantitative ADC over the resected tissue volume was obtained using NIH-Image software. The software was used to draw a region of interest around the resected tumor tissue and the mean ADC produced by this region of interest was calculated. Volumes that appeared to be cystic on the preoperative MRI were not included in this process.

Histopathologic assays

Permanent sections were prepared as described by Coons et al. [24] and subjected to quantitative analyses to determine the cell proliferative index and the cell density. Cell density was obtained from the total

nuclear counts in the field. This evaluation was made in 5–10 separate representative high power fields of each sample performed using a calibrated eyepiece graticule in a light microscope. Both the MIB-1 positive and negative nuclei were counted in an area of tissue that seemed most cell dense. The number of positive nuclei was divided by the total number of nuclei, in order to obtain the MIB-1 labeling index for cell proliferation. In selected cases, two observers independently performed nuclear counts with excellent interobserver concordance.

Statistical evaluation

The imaging and histopathological assessments were made with widely differing spatial resolution. Accordingly, we explored two candidate means of accounting for these resolution differences. One of these involved statistical regression modeling using the extreme (most abnormal) measures from imaging and histopathology. The other method used the average imaging measures over the resected volume and the average of 5–10 representative histopathological assessments of the resected tissue. To identify these representative sections, the neuropathologist qualitatively evaluated the entire sample and then chose specific fields that seemed representative of the entire sample. Quantitative assays were then performed on these fields. The latter method provided the most significant statistical correlation and is, therefore, discussed throughout the remainder of the paper. Generalized linear regression statistical modeling procedures (JMP software, SAS Institute) based on the three hypotheses were used to test for statistically significant correlations. Two different statistical regression modeling procedures were used. One procedure used a single effect regression model (e.g. nCho vs cell density, ADC vs cell density, nCho vs proliferative index). The single effect regression modeling explored the data in two ways. First, single effect regression models were constructed using the aggregate data ignoring the histopathological diagnostic classification to test for imaging-histopathology correlation over the broad spectrum of 'glioma'. Second, single effect regression models were constructed for each of the individual diagnostic classifications. Multiparametric statistical regression models using two effects, one of which was the diagnostic classification (e.g. nCho vs cell density with diagnostic classification) were also used.

Results

A representative example of imaging data is provided in Figure 1. Choline and ADC readings from each of the cases are provided in Table 1. A previously reported study (which did not include histopathology correlation) provided statistical evidence of an inverse linear correlation between ADC and nCho (data not shown). That result was reconfirmed with the present data. Single effect linear regression modeling (nCho vs ADC) gave a statistically significant negative slope (slope = -0.0072 $\pm$ 0.0022, p = 0.0046, $r^2 = 0.40$) in the plot of nCho versus ADC. This reconfirms the probability that both the nCho and the ADC are related to cell density. Representative histopathologic data is presented in Figure 2.

Correlation between choline signal and cell density

There was a statistically significant direct correlation between nCho and tumor cell density (Figure 3, Table 2). This was true when all eighteen glioma cases were considered in aggregate as well as for GBM cases alone. For diagnostic categories other than GBM, the case numbers are small and the validity of the statistical results is questionable. The alternative multiparametric regression statistical modeling procedure was also employed to explicitly take into consideration the combined influences of cell density and diagnostic classification on nCho measurements. This model (Table 3) indicates a trend ($p = 0.10$) toward a direct correlation between nCho and cell density (after the diagnostic classification effect is factored out) and, additionally, suggests a trend toward a difference in the nCho levels between GBM and oligodendroglioma (after the cell density effect is factored out). It provides no statistical support for nCho differences between GBM and lower grade astrocytoma beyond those associated with cell density.

Correlation between ADC and cell density

There was a statistically significant inverse linear correlation between the mean ADC and the cell density for glioma considered in aggregate and for GBM considered separately (Figure 4, Table 4). Table 3 provides a summary of the results of the multiparametric regression statistical modeling. This analysis showed a trend ($p = 0.07$) suggesting an inverse linear correlation

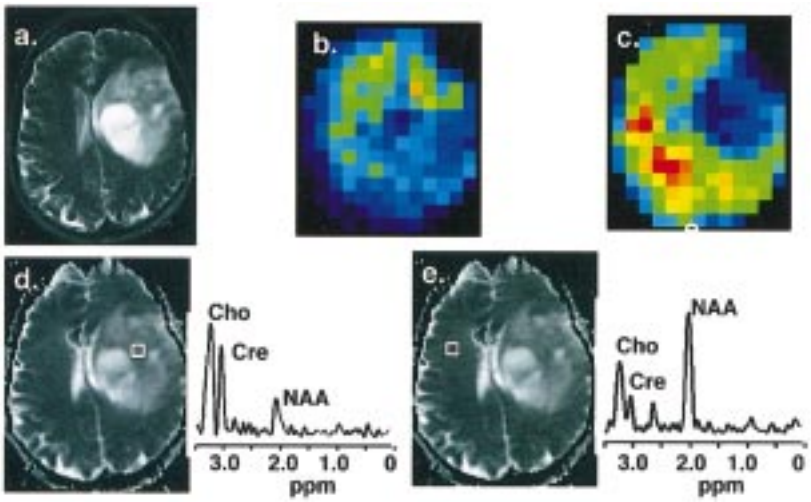

Figure 1. Representative imaging data. A single section from a case of lowgrade astrocytoma is shown. A T2-weighted MR image having a slice thickness equivalent to the spectroscopic imaging data is shown in a; b and c are the spectroscopic images. They convey the intensity of the choline signal (b) and the NAA signal (a) using identical color scales in which red represents higher signal intensity and blue represents lower signal intensity. d and e display spectra obtained from spectroscopic imaging voxels located in the tumor (d) and the normal contralateral hemisphere. The location of the voxel is displayed on an ADC image to the left of the corresponding spectra. Note the absence of NAA signal throughout the mass within which there are areas of focally elevated choline signal intensity; the greatest elevation of choline signal intensity coincides with intratumoral nodules that present relatively low intensity signal on the T2-weighted image and on the ADC image.

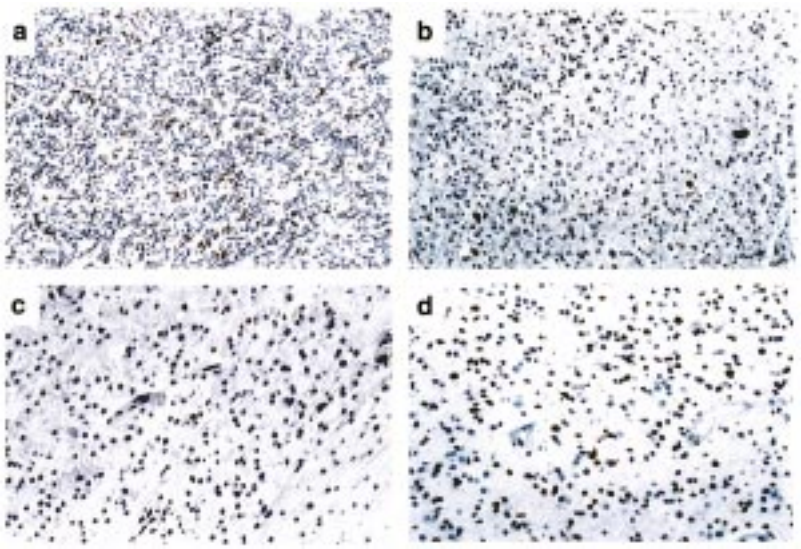

Figure 2. Representative histopathological results. Representative MIB-I immunostained sections counterstained with hematoxylin are shown at 20× magnification. The immunostaining causes the nuclei in the dividing cells to appear dark brown. a. GBM with a major oligodendroglial component (pt 17). b. Low grade oligodendroglioma (pt 8). c. Low-grade astrocytoma (pt 3). d. GBM (pt 6). Cell density and cell proliferative index differences between these four cases may be readily appreciated from qualitative inspection. Cell density, cell proliferative index, ADC, and nCho readings from these cases appear in Table 1. Note that there is a correspondence between the cell density, the ADC and nCho measures; the tumors having higher cell density tend to exhibit lower ADC readings and higher nCho readings relative to those that display lower cell density.

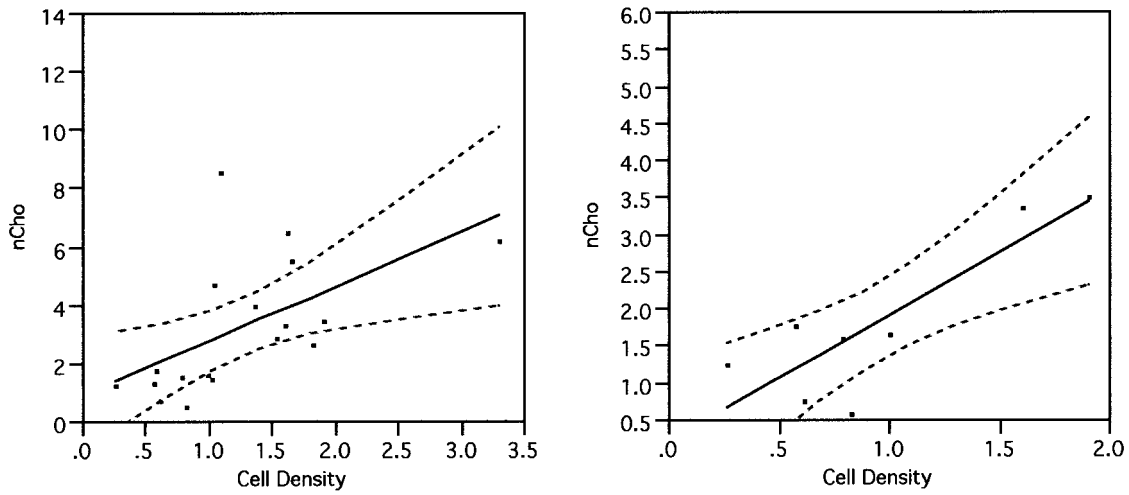

Figure 3. Summary of the relationship between nCho and cell density. The plots show one data point for each case. The units used for the x-axis are thousands of cells per high power field. The solid line is the best linear regression fit. The dotted lines convey the 95% confidence interval for the best fit. The left panel shows results from all the cases; the right panel shows results from the GBM cases only. The numerical results of the linear regression analysis are provided in Table 2. The analysis illustrates there is a statistically significant correlation between nCho and cell density for all cases considered in aggregate and for the GBM cases considered alone.

Table 2. nCho vs Cell density. Linear regression – single effect model

	N	Effect test prob > *F*	Regression slope	Slope (SE)	r^2	power
All	18	0.014	1.85	0.67	0.32	0.52
Astrocytoma	3	0.59	8.76	11.69	0.36	N.S.
GBM	8	0.007	1.71	0.42	0.73	0.55
Oligodendroglioma	4	0.8	−1.78	6.23	0.04	N.S.
Mixed	3	0.51	0.97	1.01	0.48	N.S.

between ADC and cell density (after factoring out any effects of diagnostic classification), but it failed to provide evidence for ADC differences relatable to diagnostic classifications beyond those related to cell density.

Correlation between choline and proliferative index

The single effect linear regression statistical modeling procedures provided no evidence ($p = 0.7$) for relationships between nCho and proliferative index (Figure 5). Evaluating each of diagnostic classifications separately using single effect linear regression statistical modeling provided no indication of statistically significant trends toward a correlation between nCho and proliferative index nor did multiparametric regression modeling.

Ancillary post hoc *evaluations*

Unanticipated statistically significant inverse correlations between ADC and proliferative index were found for all cases ($p = 0.009$) and for GBM alone ($p = 0.02$). These unanticipated findings may be related to the tendency for proliferating tumors to have higher cell density and, may merely restate the existence of an inverse correlation between ADC and cell density. A statistical correlation analysis showed a positive slope ($p = 0.08$) in the plot of proliferation index versus cell density (data not shown) providing some support for this argument.

Discussion

With few exceptions, investigations of human glioma which used either ^{1}H-MRSI and DI have sought to confirm clinically useful, but phenomenological, relationships between imaging measures and clinical observations. For instance, Preul et al. [25] extended numerous earlier studies on the relationship between measurable spectroscopic parameters and glioma diagnostic classification. They demonstrated that spectroscopic signal intensity patterns predict the histopathological diagnosis. This does not explain which spectroscopic signals are responsible for the discriminant power nor does it describe why the signals are altered in neoplastic tissue. The goal of this work was to study relationships between spectroscopic signals, ADC and key quantitative histopathologic variables in human glial neoplasms to relate ADC and spectroscopy results to underlying quantitative histology. Chang et al. [8] and Miller et al. [9] emphasized the influence of both cell density and proliferative potential on the choline spectroscopy signal in a study of small groups of patients having a variety of brain tumors and intracranial masses of infectious origin. The present study substantially extends upon these earlier investigations in three unique directions: (1) only primary glial tumors were studied; (2) ADC data were evaluated in addition to choline data; and (3) cell proliferative index data were evaluated in addition to cell density data. This is, to our knowledge, the only study in which the combination of choline ^{1}H-MRSI and ADC

Table 3. Statistical modeling summary: multiparametric regression model

	nCho	ADC
Overall model		
Prob > F	0.058	0.03
Power	0.66	0.73
nCho or ADC vs cell density		
Regression slope estimate	1.44	−136.00
Regression slope S.E.	0.83	68.91
Prob > $\|t\|$	0.10	0.07
Power	0.51	0.51
nCho or ADC vs diagnostic classification		
Astrocytoma–Oligodendroglioma		
Difference estimate	0.75	46.93
Difference S.E.	0.98	82.12
Prob > $\|t\|$	0.45	0.58
GBM–Oligodendroglioma		
Difference estimate	−1.35	79.54
Difference S.E.	0.75	62.76
Prob > $\|t\|$	0.10	0.23
Mixed–Oligodendroglioma		
Difference estimate	0.01	−58.64
Difference S.E.	1.04	86.63
Prob > $\|t\|$	0.99	0.51

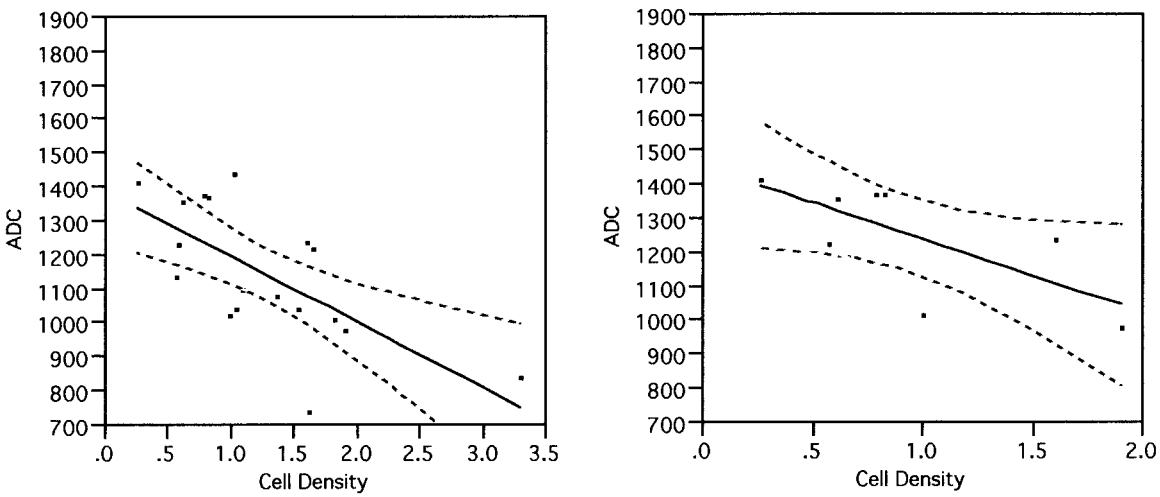

Figure 4. Summary of the relationship between ADC and cell density. One data point for each case is shown. The units used for the x-axis are thousands of cells per high power field; the units for the y-axis are (μm^2/sec). The solid line is the best linear regression fit. The dotted lines show the 95% confidence interval for the best fit. The left panel shows results from all the cases; the right panel shows result from the GBM cases only. See Table 4 for the results of the linear regression analysis. The analysis illustrates there is a statistically significant inverse correlation between ADC and cell density for all cases considered in aggregate and for the GBM cases considered alone.

Table 4. ADC vs cell density. Least squares regression – single effect model

	N	Effect test prob > *F*	Regression slope	Slope (S.E.)	r^2	Power
All	18	0.0022	−193	5.3	0.45	0.41
Astrocytoma	3	0.81	198	624	0.09	N.S.
GBM	8	0.051	−215	88	0.50	0.52
Oligodendroglioma	4	0.87	−136	753	0.016	N.S.
Mixed	3	0.12	−98	19	0.96	N.S.

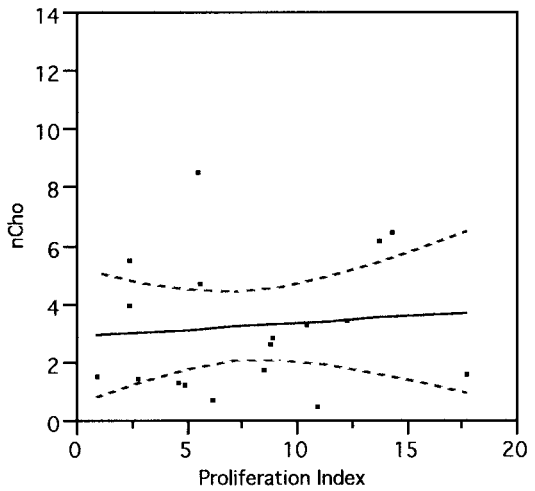

Figure 5. Summary of the relationship between nCho and cell proliferative index. The plots contain one data point for each case. The units used for the *x*-axis are percent. The solid line is the best linear regression fit. The best fit slope is not significantly different from zero as illustrated by the 95% confidence interval for the best fit (dotted lines). The analysis illustrates that there is not a statistically significant relationship between nCho and the proliferative index.

were evaluated in the context of quantitative histology for human intracranial glioma.

The findings have implications that are useful for interpreting magnetic resonance spectroscopy patterns that are seen in clinical studies of glioma. Choline containing metabolites play a central role in membrane phospholipid metabolism [14]. Therefore, their elevation in tumors often is discussed in terms of the altered membrane metabolism which accompanies neoplastic transformation. The rather imprecise term 'membrane turnover' is often used when spectroscopic findings are related to this complex metabolism. For example, several studies have shown there is a direct correlation between the choline signal and the grade of malignancy in human glioma and attributed this to elevated membrane turnover in the more malignant tissues [12,26]. However, this has not been a universal finding. Others have reported considerable variability in the choline signal measures produced by GBM [10,11]; indeed, one study suggested that GBM is characterized by lower choline signal measures compared to lower grades of malignancy [2]. These latter findings suggest that micronecrosis also influences the choline signal although, with the exception of exploratory work of Miller et al. [8,9], the relationship between choline signal and micronecrosis has not been quantitatively studied. A recent study attributed changes in choline signal following radiation therapy to the attenuation of cell proliferation and membrane turnover activity induced by the therapy [13]. Alternatively, therapeutically driven choline signal reductions might just as well be attributable to reduction in glioma cell density. Similarly the choline signal increase that coincides with recurrence or progression [4,5] may be attributable to increased cell density rather than increased cell proliferation and membrane turnover. The present finding of a direct correlation between nCho and cell density argues that one cannot attribute choline signal measures only to 'membrane turnover'; cell density is also an important factor which must be taken into consideration. Furthermore, our inability to find a relationship between cell proliferative index and the nCho suggests that cell density has a comparatively more important influence on the choline signal than does a hypothesized neoplastic acceleration of 'membrane turnover'. While we acknowledge that the inability to find a statistically significant correlation should not be taken as an evidence that it does not exist, the present findings certainly illustrate that cell density may be a more important factor than is membrane turnover.

In this study group, seven patients had either oligodendroglioma or an oligodendrocytic neoplastic component. These cases produced some of the highest nCho levels measured. The histopathologically-assessed cell density was also relatively higher in these oligodendroglial predominant lesions (Table 1). However,

even after taking the influence of cell density on the choline signal into account, the statistical analyses (Table 3) suggested a trend toward a significant difference between the nCho levels produced by oligodendroglioma and GBM after factoring out the effects of cell density. This is consistent with the *in vitro* high resolution magnetic resonance spectroscopic analyses that found a significant difference in choline signal in oligodendroglioma compared to GBM [27]. Two factors may account for apparently high choline levels seen in oligodendroglioma. First, ogliodendrocytes are responsible for myelin membrane synthesis and repair; they may, therefore, be predisposed toward having higher choline levels compared to astrocytes because of the involvement of choline metabolites in membrane metabolism. Second, the apoptotic index in oligodendroglioma is higher than GBM [28] and there are preliminary suggestions that increases in certain choline-containing metabolites are characteristic of apoptotic processes [29].

Previous imaging studies of glioma have only inferred from image evaluation that the ADC is related to tumor cell density [9,10,26]. The inference was based on the reasoning that necrotic and cystic regions have high ADC values because of the relatively large extracellular volume fraction in which diffusion is unhindered; whereas regions where there are dense masses of tumor cells produce ADC readings similar to those of normal brain tissue because there is a larger fraction of intracellular volume in which diffusion is hindered. Figure 1 illustrates these findings. There is a cystic area on the medial margin of the tumor with a central cellular area which produces a relatively low ADC signal and an elevated choline signal. Diffusion imaging has been used more frequently in the evaluation of acute ischemic stroke where a decrease in the ADC is seen to coincide with the onset of ischemia [8]. One of several interpretations of such findings is that the failure of energy production results in ion balance disturbances and the redistribution of water from the extracellular to the intracellular medium and that the volume redistribution leads to a reduced volume average ADC because diffusion in the intracellular medium is more hindered. However, the interpretation that the ADC provides a measure of the relative intracellular/extracellular volume fraction is far from widely accepted for either glioma or stroke. Therefore, we also tested the present data for a relationship between ADC and cell density. We found strong statistical evidence of an inverse linear correlation between ADC and cell density both in glioma considered in aggregate and in GBM. On the other hand, there was little evidence for differences in ADC readings between different glioma types (Table 3) even when cell density is accounted for. Our findings provide firm empirical support for the previous inferences that glioma ADC provides an independent measure of the density.

Studies involving correlation of macroscopic imaging with histopathology are limited by sampling and inherent resolution differences between techniques. In the present study these limitations were addressed as follows. The three teams (surgery, radiology and pathology) worked independently. Each team sampled and made quantitative evaluations that were representative based on their clinical experience. For instance, the radiology and pathology teams took average values over the entire available sample as being representative of the entire tumor. To increase accuracy, the radiology team evaluated imaging results only over the surgically-sampled tissue identified through comparative reading of the preoperative and postoperative imaging by an experienced radiologist. At the conclusion of these independent and clinically representative analyses, the quantitative results were subjected to statistically rigorous correlation analysis. The goal of the statistical analysis was to rule out the null hypothesis that there was no correlation between two measured parameters of interest (e.g. nCho and cell density). The analysis made this assessment through analysis of random variation in both measured parameters. We ruled out the null hypothesis because the analysis showed that there was a 95% probability that the data were not merely scattered along a horizontal line as would be seen if the null hypothesis were to be true. In our view the sampling and resolution differences between the techniques increase the degree of randomness in the measured parameters making it more difficult to rule out the null hypothesis than would be the case if the sampling and resolution differences did not exist. Negative results (failure to reject the null hypothesis) could conceivably be attributed to resolution and sampling differences limitations. For instance, the negative finding on the nCho relationship to proliferative index could be untrue. However it is unlikely that positive findings on the relationship of nCho and ADC to cell density could be the result of sampling or resolution limitations. Sampling biases can lead to unjustified rejection of the null hypothesis in correlation analyses. In this study the radiological measurements and the histopathology measurements were made by different observers who did not communicate with each other. Therefore we believe the probability of sampling

bias was small. If future technological advances result in improved spatial resolution for spectroscopic and ADC imaging or if improved methodology for prospective surgical sampling is developed, the positive results may become more probable (better *p*-values with fewer subjects) rather than less so.

Conclusion

This study used magnetic resonance spectroscopy, diffusion imaging and quantitative histopathological analyses to investigate the relationships between choline signal, ADC, cell density and cell proliferative index. We found that choline signal is directly correlated with tumor cell density and that ADC is indirectly correlated with tumor cell density, but that choline signal is not correlated with cell proliferative index. More specific statistically relevant information about other glioma subclassifications and the possible effects of prior treatment on these relationships awaits larger scale studies. These findings provide support for a self-consistent picture in which cell density is the primary biophysical factor which defines the choline signal levels and the ADCs produced by human intracranial glioma. Therefore, tumor cell density should be considered in the interpretation of clinically-indicated spectroscopic and diffusion imaging studies of glioma.

Acknowledgements

Grant support: American Cancer Society (EDT-119) to JRA. National Cancer Institute (CA 76524) to JRA. Dr. Gupta acknowledges a leave of absence from the Department of Radiology, Sanjay Gandhi Postgraduate Institute of Medical Sciences, Lucknow, India.

References

1. Duyn JH, Gillen J, Sobering G, van Zijl PC, Moonen CT: Multisection proton MR spectroscopic imaging of the brain. Radiology 188(1): 277–282, 1993
2. Fulham MJ, Bizzi A, Dietz MJ, Shih HH, Raman R, Sobering GS, Frank JA, Dwyer AJ, Alger JR, Di Chiro G: Mapping of brain tumor metabolites with proton MR spectroscopic imaging: clinical relevance. Radiology 185: 675–686, 1992
3. Lazareff JA, Olmstead C, Bockhorst KH, Alger JR: Proton magnetic resonance spectroscopic imaging of pediatric low-grade astrocytomas. Child's Nerv Syst 12: 130–135, 1996
4. Tedeschi G, Lundbom G, Raman R, Bonavita S, Duyn JH, Alger JR, Di Chiro G: Increased choline signal coinciding with malignant degeneration of cerebral gliomas: a serial proton magnetic resonance spectroscopy imaging study. J Neurosurg 8: 516–524, 1997
5. Wald LL, Nelson SJ, Dey MR, Noworolski SE, Henry RG, Huhn SL, Chang S, Prados MD, Sneed PK, Larson DA, Wara WM, McDermott M, Dillon WP, Gutin PH, Vigneron DB: Serial proton magnetic resonance spectroscopy imaging of glioblastoma multiforme after brachytherapy. J Neurosurg 87: 525–534, 1997
6. Go KG, Keuter EJ, Kamman RL, Pruim J, Metzemaekers JD, Staal MJ, Paans AM, Vaalburg W: Contribution of magnetic resonance spectroscopic imaging and L-[1-11C]tyrosine positron emission tomography to localization of cerebral gliomas for biopsy. Neurosurgery 34: 994–1002, 1994
7. Alger JR, Frank JA, Bizzi A, Fulham MJ, DeSouza BX, Duhaney MO, Inscoe SW, Black JL, van Zijl PC, Moonen CT, Di Chiro G: Metabolism of human gliomas: assessment with H-1 MR spectroscopy and F-18 fluorodeoxyglucose PET. Radiology 177: 633–641, 1990
8. Chang L, McBride D, Miller BL, Cornford M, Booth RA, Buchthal SD, Ernst TM, Jenden D: Localized |it in vivo 1H magnetic resonance spectroscopy and *in vitro* analyses of heterogeneous brain tumors. J Neuroimaging 5:157–163, 1995
9. Miller BL, Chang L, Booth R, Ernst T, Cornford M, Nikas D, McBride D, Jenden DJ: *In vivo* 1H MRS choline: correlation with *in vitro* chemistry/histology. Life Sci 58: 1929–1935, 1996
10. Negendank WG, Sauter R, Brown TR, Evelhoch JL, Falini A, Gotsis ED, Heerschap A, Kamada K, Lee BC, Mengeot MM, Moser E, Padavic-Shaller KA, Sanders JA, Spraggins TA, Stillman AE, Terwey B, Vogl TJ, Wicklow K, Zimmerman RA: Proton magnetic resonance spectroscopy in patients with glial tumors: a multicenter study. J Neurosurg 84: 449–458, 1996
11. Ott D, Hennig J, Ernst T: Human brain tumors: assessment with *in vivo* proton MR spectroscopy. Radiology 186: 745–752, 1993
12. Speck O, Thiel T, Hennig J: Grading and therapy monitoring of astrocytomas with 1H-spectroscopy: preliminary study. Anticanc Res 16: 1581–1585, 1996
13. Sijens PE, Vecht CJ, Levendag PC, van Dijk P, Oudkerk M: Hydrogen magnetic resonance spectroscopy follow-up after radiation therapy of human brain cancer. Unexpected inverse correlation between the changes in tumor choline level and post gadolinium magnetic resonance imaging contrast. Invest Radiol 30: 738–744, 1995
14. Aiken NR, Gillies RJ: Phosphomonoester metabolism as a function of cell proliferative status and exogenous precursors. Anticanc Res 16: 1393–1397, 1996
15. Le Bihan D: Molecular diffusion nuclear magnetic resonance imaging. Magn Reson Q 7: 1–30, 1991
16. Baird A, Warach S: Magnetic Resonance Imaging of acute stroke. J Cereb Blood Flow Metab 18: 583–609, 1998
17. Brunberg JA, Chenevert TL, McKeever PE, Ross DA, Junck LR, Muraszko KM, Dauser R, Pipe JG, Betley AT: *In vivo*

MR determination of water diffusion coefficients and diffusion anisotropy: correlation with structural alteration in gliomas of the cerebral hemispheres. Am J Neuroradiol 16: 361 – 371, 1995
18. Krabbe K, Gideon P, Wagn P, Hansen U, Thomsen C, Madsen F: MR diffusion imaging of human intracranial tumors. Neuroradiology 39: 483–489, 1997
19. Le Bihan D, Douek P, Argyropoulou M, Turner R, Patronas N, Fulham M: Diffusion and perfusion magnetic resonance imaging in brain tumors. Top Magn Reson Imag 5: 25–31, 1993
20. Tien RD, Felsberg GL, Friedman H, Brown M, MacFall J: MR imaging of high grade cerebral gliomas: value of diffusion weighted echoplanar pulse sequences. Am J Roentgenol 162: 671–677, 1993
21. Gupta RK, Sinha U, Cloughesy TF, Alger JR: Inverse correlation between choline magnetic resonance spectroscopy signal intensity and the apparent diffusion coefficient in human glioma. Magn Reson Med 41: 2–7, 1999
22. Yanaka K, Shirai S, Kimura H, Kamezaki T, Matsumuna A, Nose T: Clinical application of diffusion-weighted magnetic resonance imaging to intracranial disorders. Neurol Med Chr (Tokyo) 35: 648–654, 1995
23. Daumas-Duport C, Scheithauer B, O'Fallon J, Kelly P: Grading of astrocytomas: a simple and reproducible method. Cancer 62: 2152–2165, 1988
24. Coons SW, Johnson PC: Regional heterogeneity in the proliferative activity of human gliomas as measured by the Ki-67 labeling index. J Neuropath Exp Neurol 52: 609–618, 1993
25. Preul MC, Caramanos Z, Collins DL, Villemure JG, Leblanc R, Olivier A, Pokrupa R, Arnold DL: Accurate, noninvasive diagnosis of human brain tumors by using proton magnetic resonance spectroscopy. Nature Med 2: 323–325, 1996
26. Gill SS, Thomas DG, Van Bruggen N, Gadian DG, Peden CJ, Bell JD, Cox IJ, Menon DK, Iles RA, Bryant DJ: Proton MR spectroscopy of intracranial tumours: *in vivo* and *in vitro* studies. J Comp Assist Tomogr 14: 497–504, 1990
27. Carapella CM, Carpinelli G, Knijn A, Raus L, Caroli F, Podo F: Potential role of *in vitro* 1H magnetic resonance spectroscopy in the definition of malignancy grading of human neuroepithelial brain tumours. Acta Neurochirurgica (Supple.) 68: 127–132, 1997
28. Schiffer D, Cavalla P, Migheli A, Chió A, Giordana MT, Marino S, Attanasio A: Apoptosis and cell proliferation in human neuroepithelial tumors. Neurosci Lett 195: 81–84, 1995
29. Nunn AV, Barnard ML, Bhakoo K, Murray J, Chilvers EJ, Bell JD: Characterisation of secondary metabolites associated with neutrophil apoptosis. FEBS Lett 392: 295–298, 1996

Address for offprints: Jeffry R. Alger, Department of Radiological Sciences, UCLA Medical Center, BL-428 CHS, l0833 Le Conte Avenue, Los Angeles, CA 90095-1721, USA; Tel.: (310) 206-3344; Fax: (310) 794-7406; E-mail: jralger@ucla.edu